Acta Crystallographica Section D
Biological Crystallography
ISSN 0907-4449

Atomic resolution structures of ribonuclease A at six pH values

R. Berisio,[a]† F. Sica,[b]† V. S. Lamzin,[c] K. S. Wilson,[d] A. Zagari[e] and L. Mazzarella[b]*

[a]Centro di Studio di Biocristallografia, CNR, Via Mezzocannone 6, I-80134 Napoli, Italy, [b]Dipartimento di Chimica, Università degli Studi di Napoli 'Federico II', Complesso Universitario di Monte Sant'Angelo, Via Cinthia, I-80126 Napoli, Italy, [c]European Molecular Biology Laboratory (EMBL) c/o DESY, Notkestrasse 85, D-22603 Hamburg, Germany, [d]Department of Chemistry, University of York, Heslington, York YO1 5DD, England, and [e]Dipartimento di Chimica Biologica, Università degli Studi di Napoli 'Federico II', Via Mezzocannone 6, I-80134 Napoli, Italy

† RB and FS contributed equally to this work.

Correspondence e-mail: mazzarella@chemistry.unina.it

Received 10 October 2001
Accepted 19 December 2001

PDB References:
ribonuclease A, pH 5.2, 1kf2, r1kf2sf; ribonuclease A, pH 5.9, 1kf3, r1kf3sf; ribonuclease A, pH 6.3, 1kf4, r1kf4sf; ribonuclease A, pH 7.1, 1kf5, r1kf5sf; ribonuclease A, pH 8.0, 1kf7, r1kf7sf; ribonuclease A, pH 8.8, 1kf8, r1kf8sf.

The diffraction pattern of protein crystals extending to atomic resolution guarantees a very accurate picture of the molecular structure and enables the study of subtle phenomena related to protein functionality. Six structures of bovine pancreatic ribonuclease at the pH* values 5.2, 5.9, 6.3, 7.1, 8.0 and 8.8 and at resolution limits in the range 1.05–1.15 Å have been refined. An overall description of the six structures and several aspects, mainly regarding pH-triggered conformational changes, are described here. Since subtle variations were expected, a thorough validation assessment of the six refined models was first carried out. Some stereochemical parameters, such as the $N-C^{\alpha}-C$ angle and the pyramidalization at the carbonyl C atoms, indicate that the standard target values and their weights typically used in refinement may need revision. A detailed comparison of the six structures has provided experimental evidence on the role of Lys41 in catalysis. Furthermore, insights are given into the structural effects related to the pH-dependent binding of a sulfate anion, which mimics the phosphate group of RNA, in the active site. Finally, the results support a number of thermodynamic and kinetic experimental data concerning the role of the disulfide bridge between Cys65 and Cys72 in the folding of RNase A.

1. Introduction

Proteins can be regarded as assemblies of amino-acid residues, with different acid/base properties, which are kept together by a delicate balance of forces. Consequently, the reactions of proteins to pH changes are not easily predictable. For example, many proteins are catalytically active only in a tiny pH range and/or their stability is strongly pH-dependent. Since several protein functional properties are very sensitive to pH changes, such as substrate binding, stability, catalytic efficiency and others, it is intriguing to understand what happens at a structural level. Therefore, it is not surprising that several studies of the relationship between protein conformation and pH have been carried out (Dixon *et al.*, 1991; Gursky *et al.*, 1992; Yang & Phillips, 1996). Among these, the crystallographic study of sperm whale myoglobin at three different pH values (Yang & Phillips, 1996) has highlighted the way this parameter influences ligand binding through the distal and proximal histidines. Until very recently, these studies were restricted by the resolution often being limited to around 2.0 Å, where the uncertainty in refined atomic co-ordinates is large enough to obscure the possible significance of many local differences between two models.

Atomic resolution studies have recently proved to be able to highlight even very subtle features which may have an important role in protein functionality (Dauter *et al.*, 1997; Esposito, Vitagliano, Zagari *et al.*, 2000). For studies of the

protein conformational dependence upon pH, the biological relevance of obtaining atomic resolution models arises from the desire to identify significant differences between similar structures. Only very recently have atomic resolution studies been carried out to investigate the detailed structural effects of pH variation. The atomic resolution structure of the core domain of avian sarcoma virus integrase (Lublowski *et al.*, 1999), determined at pH 6.0 and 7.5, has allowed the explanation of the pH dependence of its activity, showing that a basic pH induces disorder in the catalytic loop.

We have studied the structure of bovine pancreatic ribonuclease (RNase A) at six pH values and at a resolution close to 1 Å. RNase A is an endoribonuclease that cleaves and hydrolyzes single-stranded RNA in two distinct steps (Blackburn & Moore, 1982). In the first step, the 3′–5′ phosphate linkage of RNA is cleaved *via* intramolecular transphosphorylation, leading to a 2′–3′ cyclic phosphate intermediate. In the second step, the cyclic phosphate is hydrolized by a water molecule to produce a 3′ monophosphate ester. His12 and His119 are proposed to act as the general base and the general acid, respectively, in the first step and they reverse their roles in the second step (Blackburn & Moore, 1982). Lys41 is thought to stabilize the reaction intermediate, although its role in catalysis is still under debate (Wladkowski *et al.*, 1998).

In a previous report, we mainly focused on the protonation equilibrium involving the catalytic histidine residues. Furthermore, we showed that atomic resolution is able to provide an estimate of the pK_a values of residues by following the changes of some specific protein stereochemical parameters (Berisio *et al.*, 1999). The six models at pH* values 5.2, 5.9, 6.3, 7.1, 8.0 and 8.8 (Berisio *et al.*, 1999), which have here been re-refined for a better description of the solvent structure, are the highest resolution so far known for RNase A.

This work reports a comprehensive description of the overall RNase A structures and a number of new structural details extracted from a comparative analysis of the six refined models, together with their possible biological implications.

Table 1
Statistics of the refinement.

The DELU, ISOR and SIMU restraints are defined in §2.

pH*	5.2	5.9	6.3	7.1	8.0	8.8
Resolution (Å)	1.10	1.05	1.10	1.15	1.15	1.15
Reflections	46613	53494	47420	42225	41956	41615
Rejection criteria	None					
R factor for all data	0.103	0.102	0.104	0.106	0.106	0.106
R factor for $F > 4\sigma$	0.098	0.099	0.099	0.103	0.100	0.100
Protein atoms (partially occupied)	1053 (198)	1047 (186)	1049 (193)	1055 (207)	1044 (181)	1049 (192)
Water molecules (partially occupied)	248 (110)	246 (98)	230 (90)	237 (94)	232 (85)	236 (93)
Sulfate ion occupancy	0.8	0.3	0.2	0.0	0.0	0.0
Side chains in multiple conformations	21	21	21	21	20	21
R.m.s. deviations from ideal geometry						
Bond distances (Å)	0.015	0.016	0.018	0.015	0.016	0.016
Angle distances (Å)	0.038	0.032	0.035	0.033	0.032	0.033
Chiral volumes (Å^3)	0.152	0.152	0.151	0.140	0.156	0.156
Anisotropic displacement parameters (U_{ij}) r.m.s. deviations						
DELU (Å^2)	0.027	0.006	0.011	0.006	0.006	0.007
ISOR (Å^2)	0.028	0.031	0.024	0.024	0.024	0.028
SIMU (Å^2)	0.078	0.072	0.078	0.082	0.079	0.081
Average main-chain positional uncertainties (Å)	0.021	0.015	0.017	0.020	0.021	0.021
Most favoured (additionally allowed) φ/ψ (%)	90.4 (9.6)	93.0 (7.0)	92.1 (7.9)	93.0 (7.0)	91.2 (8.8)	93.0 (7.0)

2. Materials and methods

2.1. Structure refinements

We reported previously the procedure for crystallization, soaking of the crystals at the six pH* values and data collection (Berisio *et al.*, 1999). pH* stands for the apparent proton activity of aqueous–organic solutions (Tilton *et al.*, 1992; Berisio *et al.*, 1999). The structures reported by Berisio *et al.* (1999) were re-refined using *SHELXL* in order to obtain a more accurate modelling of the solvent structure. Indeed, compared with these structures, attention was paid to the modelling of water molecules in terms of alternative networks around the protein surface. During this modelling, more restrictive criteria in the attribution of the water peaks were used, despite a small increase in the *R* factor.

Bond distances and bond angles were restrained with target σ values of 0.02 and 0.04 Å, respectively (angles were treated as 1,3-distances). The planarity of the peptide bond was restrained by setting to zero the chiral volume of the two polyhedrons having O—C$^\alpha$—N(+1)—C$^\alpha$(+1) and O—C$^\alpha$—N(+1)—C atoms as corners, with a σ value of 0.5 Å^3. Chiral volumes were restrained using a σ value of 0.2 Å^3. Bonded atoms were restrained to have similar atomic displacement parameters with an effective standard deviation of 0.2 Å^2. For each pair of chemically bonded atoms, the components of the anisotropic displacement parameters along the 1,2- and 1,3-vector directions were restrained to be equal (DELU restraint) with a standard deviation of 0.01 Å^2. Furthermore, the components of spatially close atoms were restrained to be the same (SIMU restraint) with a standard deviation of 0.2 Å^2. An attempt to relax the restraints was not successful, since it produced deterioration of the model geometry. Atomic displacement parameters for H atoms were set to 1.2 times the B_{eq} of the atoms they were bound to. The water sites were restrained to adopt an approximately isotropic behavior (ISOR restraint). Those in proximity to protein residues in multiple conformations were refined with occupancies restrained to those of the appropriate side chain using the SUMP option in *SHELXL* (Sheldrick & Schneider, 1997). Full occupancies were reset to 0.5 for water molecules having B_{eq}

greater than 65 Å^2 and refinement continued. Water sites having half occupancies and B_{eq} greater than 65 Å^2 were then rejected. Refinement cycles were alternated with careful inspections of the $(3F_o - 2F_c)$ and the omit $(F_o - F_c)$ electron-density maps using the program *O* (Jones *et al.*, 1991).

The models refined to *R* factors ranging from 0.102 to 0.106. Estimated uncertainties of the atomic positions were derived using block-matrix least-squares refinement as implemented in *SHELXL* (Scheldrick & Schneider, 1997). For block-matrix refinement, the model was split into five overlapping blocks containing approximately the same number of atoms. Since a slight underestimation of the e.s.d. values may arise from the use of the restraints, most of them were removed during refinement, thus providing more reliable estimates of the errors. Final statistics of the refinement are reported in Table 1.

2.2. Electrostatic calculations

Electrostatic potential calculations were carried out by solving the non-linear Poisson–Boltzmann equation using the finite difference method implemented in the program *DELPHI* (Nicholls & Honig, 1991). Calculations were carried out on a 0.91 Å grid spacing and no water molecules were explicitly included in the crystal structure. An interior dielectric constant of 4 and an exterior dielectric constant of 80 (Gilson & Honig, 1987) were used. Potentials were displayed on the accessible surface, as calculated by *GRASP*, with a solvent probe radius of 1.4 Å (Nicholls & Honig, 1991).

The contributions of charged residues to the electrostatic potential $\varphi(r)$ at Lys41 were related to the pK_a shifts by the simple relation $\Delta pK_a = \Delta\varphi/2.3RT$ (Honig & Nicholls, 1995). The change of the long-range charge–charge interaction energy between Lys41 and the surrounding charged residues was calculated as $\Delta\Delta G = 5.7 \times \Delta pK_a$ kJ mol^{-1}.

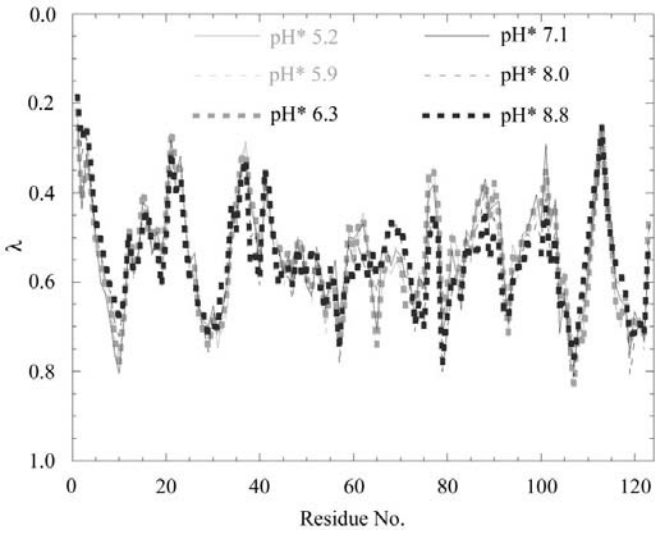

Figure 1
Anisotropy factor λ averaged over the main-chain atoms within each residue *versus* residue number for the six models at the six pH*; the lowest λ values in the plot correspond to loop regions.

3. Results and discussion

3.1. The quality of the models

Six structures of RNase A at pH* 5.2, 5.9, 6.3, 7.1, 8.0 and 8.8, refined at similar resolution limits resulted in six models of comparable accuracy. Uncertainties in the atomic positions of the six structures averaged over the main-chain atoms are all of the order of 0.02 Å (Table 1).

As shown in Fig. 1, the anisotropy factors λ, calculated as the ratio between the minimum and the maximum eigenvalue of the U_{ij} atomic displacement parameter matrix, are independent of pH. In contrast, they strongly depend upon residue location, with higher values for the external loops. The strong similarity of the anisotropy factors of all six structures is noteworthy and reflects the high level of accuracy of the refined models (Fig. 1).

Several residues in multiple conformations could be modelled (Table 1), in particular at the protein surface. In addition, ionizable residues (His119 and Lys41) or residues with their conformations influenced by neighbouring ionizable residues (Lys7, Gln11 and Gln101) show clear pH*-correlated changes in their occupancies, with one predominant conformer at low pH* giving way to a different conformer at high pH*. In contrast, the occupancies of non-ionizable residues are comparable in all the six structures.

The final difference electron-density maps contoured at 1.6–2.6σ revealed many H atoms, even before their contribution was introduced in the structure-factor calculation. At the end of the refinement, H atoms were omitted from the structure-factor calculation and ten additional cycles of refinement were carried out before omit map checks. H atoms were classified on the basis of the secondary-structure elements their bound atoms belonged to. Most of the H atoms on atoms in β-strand (98% on main-chain and 35% on side-chain atoms in the representative structure at pH* 5.9) or α-helical conformations (95% on main-chain atoms and 35% on side-chain atoms) were clearly detectable, whereas a smaller number of H atoms was detected in the loop regions (75% on main-chain and 31% on side-chain atoms).

3.2. Conformation and geometry

The availability of six independently refined structures provided valuable validation tools to assess the significance of subtle structural features, in particular in the protein main chain. Indeed, the distribution of N—C$^\alpha$—C angles and of the pyramidalization angles at the carbonyl C atoms were analyzed to exhaustively validate the six final models.

3.2.1. N—C$^\alpha$—C analysis. *Ab initio* calculations, along with statistics on small molecules (Ashida *et al.*, 1987) and on protein structures (Karplus, 1996), have shown that residues adopting an extended conformation, such as β-strands, are characterized by a larger N—C$^\alpha$—C angle than residues in α-helices. For example, we have recently found a strict dependence of the geometry of the residues on protein conformation for a deamidated form of RNase A determined at 0.87 Å resolution (Esposito, Vitagliano, Sica *et al.*, 2000).

The distribution of N—C^{α}—C angles was analyzed for the six final RNase A models. Residues in secondary-structure elements were selected according to Kabsch & Sander (1983). Although the same target value was used (111.2°) for the refinement of the whole structure, different distributions of the N—C^{α}—C angles were found for residues adopting α-helix and those adopting β-strand conformations. In particular, the mean values of N—C^{α}—C angles after averaging over the six models were 109.5 and 111.6° for α-helices and β-strands, respectively (Figs. 2*a* and 2*b*). Such a difference of about 2° is significant given the low e.s.d. values for bond angles of about 0.6°. Among the residues in α-helical conformation, the catalytic His12, which is located at the terminal part of the N-terminal helix, shows the largest deviation from the mean.

3.2.2. Pyramidalization. Theoretical calculations on small molecules indicate that local effects may induce pyramidalization at the main-chain carbonyl C atom (Jeffrey *et al.*, 1985). Such pyramidalization may be defined as a distortion of the peptide group from planarity, which produces a partially staggered conformation about the C^{α}—C bond and can be quantitatively described by the angle

$$\theta = \omega(C_i^{\alpha}C_iNC_{i+1}^{\alpha}) - \omega'(OC_iNC_{i+1}^{\alpha}) + \pi(\mathrm{mod}2\pi).$$

In the absence of pyramidalization, the θ angle is zero. By analysis of nine ultrahigh resolution structures, we have recently demonstrated that this effect occurs in protein structures (Esposito, Vitagliano, Zagari *et al.*, 2000).

In agreement with these results, we found an appreciable degree of pyramidalization in all six RNase A models, despite the use of the planarity restraints for the peptide groups during refinement. Peptide planes were selected on the bases of their B_{eq}, in order to only use measurements from well defined regions (Fig. 2*c*).

Fig. 2(*c*) shows that pyramidalization, averaged over the corresponding peptide groups of the six models, clearly depends upon the protein backbone conformation. In particular, positive values of the θ angle are observed for residues adopting α-helical conformation, whereas negative values are adopted by residues in the extended conformation, with an average θ value of 1.0 and −2.1° for ψ ranging from −60 to 0° and from 120 to 180°, respectively (Fig. 2*c*). The conformational dependence of the θ angle can be seen in each of the six structures, with a strong correlation between the corresponding peptide groups (correlation factors ranging from 0.71 to 0.85).

3.3. Conformational mobility in the catalytic site

The catalytic site of RNase A is mainly composed of His12, His119, Gln11, Lys41 and Asp121. Of these residues, His119, Gln11 and Lys41 adopt double conformations, whereas His12 and Asp121 adopt single conformations, as they are tightly anchored to the protein backbone. The effect of the protonation state of the catalytic histidines on their conformation has previuosly been discussed (Berisio *et al.*, 1999). Similar to His119, the conformations of Lys41 and Gln11 are pH dependent and their occurrence is correlated to the release of a sulfate ion from the active site at neutral pH* (Table 1).

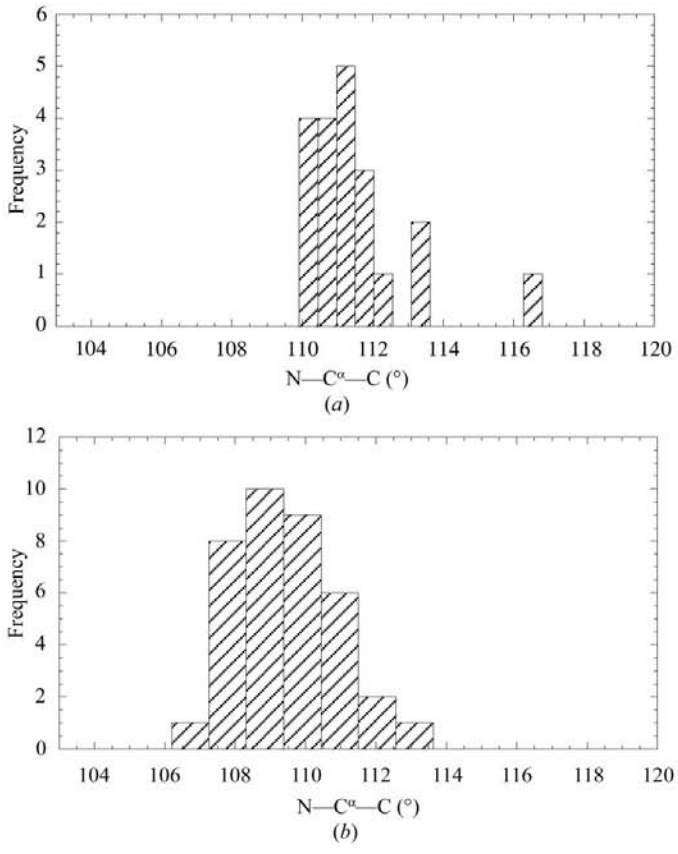

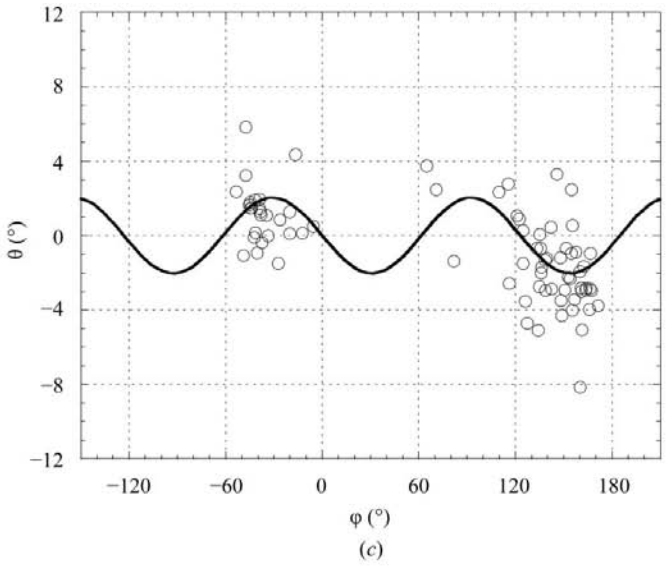

Figure 2
N—C^{α}—C angles averaged over the six models for residues in (*a*) α-helix and (*b*) β-strand conformations. (*c*) Pyramidalization angles (θ) at the carbonyl C atoms. The θ angles averaged over the six structures are plotted against the backbone ψ angle and the data are interpolated using a threefold function. 76 peptide planes were selected having B_{eq} of the carbonyl O atoms (B_{eq}O) lower than ($\langle B_{eq}\mathrm{O}\rangle + 0.1\langle B_{eq}\mathrm{O}\rangle$).

Fig. 3(*a*) shows a superimposition of the structures at pH* 5.2 and 8.0, with only the predominant conformers at each pH* shown for clarity. In the pH* range 5.2–8.0 the *A* and *B* conformers of Gln11 are related essentially by a rotation χ_1, whereas the two conformations of Lys41 differ in the orientation of N^{ζ}. At the lower limit of this pH* range (5.2–6.3), the sulfate ion in the active site is bound to Lys41*A* and to Gln11*A* and cannot coexist with Gln11*B* (Fig. 3*a*). Gln11*B* still occurs with a low occupancy at acidic pH*, since the occupancy of the sulfate site is less than one even at pH* 5.2. In accordance with the literature data (Tilton *et al.*, 1992; Wlodawer *et al.*, 1988), both Gln11 and Lys41 strongly prefer the *A* conformation in the presence of sulfate (with occupancies of 80%). In the *A* conformation, Lys41 is also stabilized by hydrogen-bonding interactions with Asn44 $O^{\delta1}$ (Fig. 3*a*). The sulfate anion is progressively released with pH* and water molecules occupy the active site at pH* 7.1. Furthermore, the *B* conformations of both Gln11 and Lys41 become predominant. In the *B* conformation, Lys41 maintains its interaction with Asn44 $O^{\delta1}$ and forms a new interaction with the carbonyl group of Val43 (Fig. 3*a*).

In the pH* range 8.0–8.8 another conformational variation occurs (Figs. 3*b* and 3*c*). Indeed, Lys41 adopts two conformations, both directed away from the active site. This conformational change of Lys41 is correlated to the structural reorganization of the *B* conformer of Gln11 to form a hydrogen bond with Asn44 $O^{\delta1}$ (Figs. 3*b* and 3*c*). We attribute these changes to the deprotonation of Lys41, which weakens its hydrogen-bonding interactions with Asn44 and Val43. The deprotonation of Lys41 requires its pK_a to be peculiarly low. An unusually low value of pK_a of 8.9 had previously been found for Lys41 in solution (Knoblauch *et al.*, 1988). As shown by the electrostatic potential at the protein surface, calculated at the two extremes of pH*, the active site is left nearly uncharged at basic pH*, whereas a positively charged area generated by Lys7, Arg10 and Arg39 is still present (Figs. 4*a* and 4*b*).

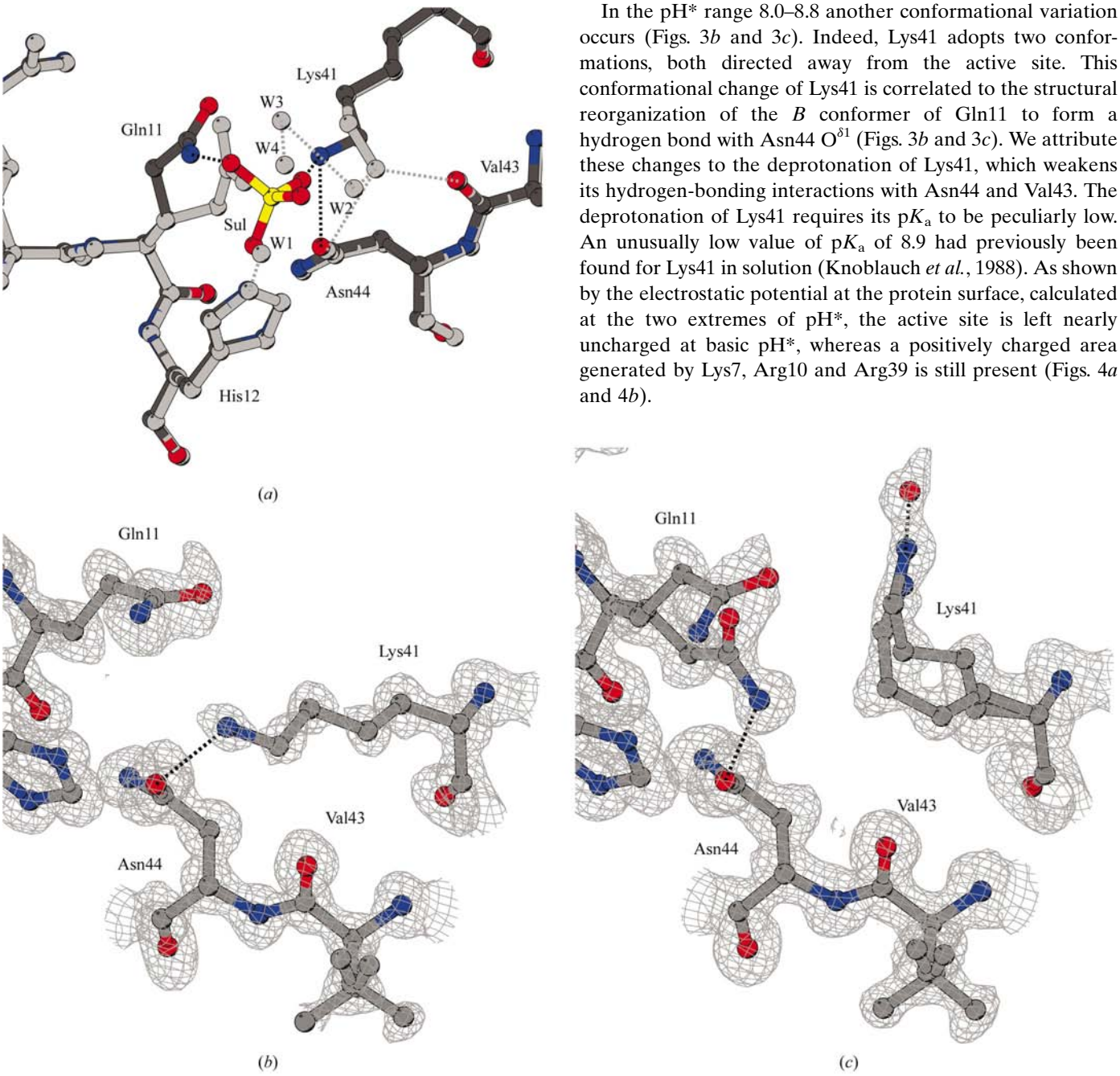

Figure 3
Conformational changes of the catalytic Gln11 and Lys41. (*a*) Superposition of the two structures at pH* 5.2 (dark grey) and 8.0 (light grey); only the most populated conformers are shown for clarity. (*b*) Electron-density maps ($3F_o - 2F_c$) contoured at 1.7σ for the structures at pH* 5.2 and (*c*) at pH* 8.8. The figures were generated using the program *BOBSCRIPT* (Esnouf, 1999).

By solving the Poisson–Boltzman equation using the *DELPHI* program (Honig & Nicholls, 1995), the contribution of each residue to the electrostatic potential at Lys41 was derived with the structure at pH* 8.0 used as a template and the pK_a shift from the canonical value was calculated. As shown in Table 2, Arg10, Lys66, Lys7 and Arg39 are the residues contributing the most to depress the pK_a of Lys41. An overall pK_a shift of −1.5 pK units, corresponding to a destabilization of the protonated Lys41 of about 8.4 kJ mol^{-1}, was calculated. This compares well with the measured pK_a of 8.9 in solution (Knoblauch *et al.*, 1988). For comparison, pK_a shifts were calculated also for the other lysines in the structure and no significant pK_a shift was found, apart from Lys7 (pK_a shift −1.2 units), which is the closest to Lys41 (Fig. 4*a*).

A pK_a shift was calculated also for the conformations adopted by Lys41 at pH* 8.8. Both conformations of Lys41 occurring at pH* 8.8 move closer to the positively charged region shown in Fig. 4(*b*). Therefore, it is not surprising that the pK_a of Lys41 is further depressed in these new conformations, as ΔpK_a is −3.1 units and the protonated Lys41 is destabilized by about 17.6 kJ mol^{-1} owing to unfavourable charge–charge interactions.

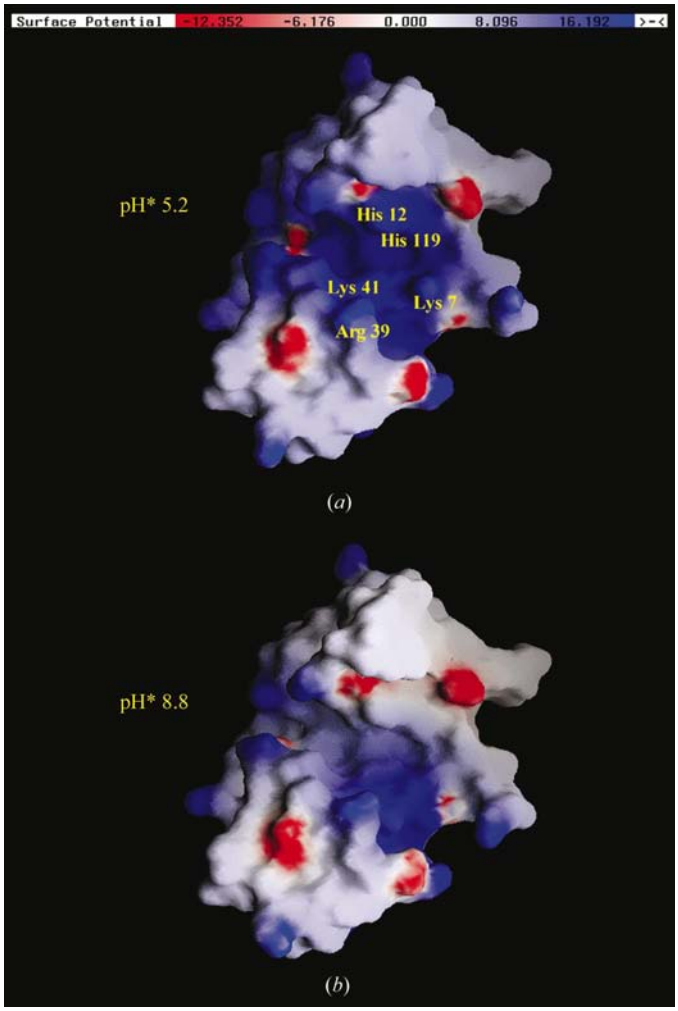

Figure 4
(*a*) Electrostatic potential at the protein surface calculated using *DELPHI* at pH* 5.2 and (*b*) at pH* 8.8. The figures were generated using *GRASP* (Nicholls & Honig, 1991).

Table 2
Contribution of charged residues to the pK_a shift of Lys41 (pK units).

Only the most abundant conformer was considered for residues in multiple conformations.

Negatively charged groups		Positively charged groups	
Residue	ΔpK_a	Residue	ΔpK_a
		N-term	−0.15
Glu2	0.29	Lys1	−0.23
Glu9	0.16	Lys7	−0.60
Asp14	0.21	Arg10	−0.51
Asp38	0.30	Lys31	−0.15
Glu49	0.13	Arg33	−0.38
Asp53	0.10	Lys37	−0.21
Asp83	0.55	Arg39	−0.66
Glu86	0.34	Lys61	−0.10
Glu111	0.26	Lys66	−0.45
Asp121	0.48	Arg85	−0.41
OXT	0.19	Lys91	−0.13
		Lys98	−0.16
		Lys104	−0.25

3.3.1. Implications for the role of Lys41 in the catalytic mechanism. Despite the progress made in characterizing several aspects of the RNase A reaction mechanism, many questions regarding the role of Lys41 in catalysis still remain open. Lys41 is often proposed as an electrostatic catalyst that stabilizes the anionic reaction intermediate through electrostatic interactions (Blackburn & Moore, 1982). Recently, Wladkowski *et al.* (1998) have proposed that Lys41 may act as a general base instead of His12 in RNA cleavage.

Our structures show that, in its protonated state, Lys41 points towards the active site both in the presence and in the absence of sulfate (Fig. 3*a*), despite the existence in the latter case of a highly positive electrostatic potential in the active site at acidic pH* (Fig. 4*a*). Indeed, there is an appreciable occupancy of the protonated Lys41 in the *B* conformation that is not compatible with the existence of a sulfate anion in the active site. Furthermore, at pH* 8.8 Lys41 is positioned far from the active site, as the distance from His12 $N^{\varepsilon 2}$ to Lys41 N^{ζ} is close to 8.5 Å. The conformational change observed together with the electrostatic calculations indicate that the deprotonation of Lys41 occurs in the pH* range 8.0–8.8. In conflict with the proposal of Wladkowski *et al.* (1998), this finding suggests that Lys41 is unlikely to remain unprotonated in the active site at neutral pH and, therefore, to act as a general base during catalysis. In addition, the presence of the negatively charged substrate would act to increase the pK_a of Lys41, which would become an even worse candidate to act as a general base in the mechanism.

As shown in Table 2, Lys7 and Arg10, which belong to the P2 phosphate-binding subsite, play a major role in depressing the pK_a of Lys41. The P2 subsite of RNase A hosts the phosphate group adjacent to the 3′ side of the phosphate in the active site. Site-directed mutagenesis has shown that P2 induces an enhanced catalytic efficiency of the enzyme not only in the case of polynucleotides, but also for the low molecular mass cytidine 2′,3′-cyclic phosphate, which does not

bind to the P2 subsite (Nogues *et al.*, 1998). Our experiment confirms the idea that electrostatic interactions with Lys7 and Arg10 are important for catalysis and is in accordance with mutagenesis studies (Fisher, Ha *et al.*, 1998; Fisher, Schultz *et al.*, 1998). In addition, it suggests that these residues enhance catalysis by limiting the conformational flexibility of Lys41. Indeed, all conformations pointing towards the P2 subsite, rather than towards the active site, are strongly destabilized when Lys41 is charged.

Furthermore, Table 2 shows that Arg39 contributes substantially to the electrostatic potential at Lys41. However, it has been shown by mutagenesis studies that Arg39 does not contribute to catalysis, despite its proximity to the P2 subsite (Fisher, Grilley *et al.*, 1998). In our structures, Arg39 does not form any intramolecular contacts and its conformation is driven by electrostatic interactions with the Glu111 of a symmetry-related molecule. The side chain of Arg39 preferentially adopts a fully exposed conformation in solution (Santoro *et al.*, 1993). In this conformation, the contribution of Arg39 to the electrostatic potential at Lys41 was found to be negligible. This finding reconciles our results with the literature data and, in addition, emphasizes the importance of using the correct model for electrostatic calculations. Indeed, residues involved in crystal packing interactions should be critically analyzed and in some cases excluded when the results are meant to be extrapolated to the situation in solution.

3.4. Structural changes arising from ligand binding

The pH dependence of ligand binding to RNase A is largely governed by the catalytic histidines (Park *et al.*, 2001). Consistent with this finding, our data show that the sulfate ion bound to the catalytic His12, His119 and Lys41, which mimics the phosphate group of RNA, is released with an increase of pH*. Furthermore, sulfate binding is accompanied by subtle yet systematic changes of the tertiary structure of RNase A.

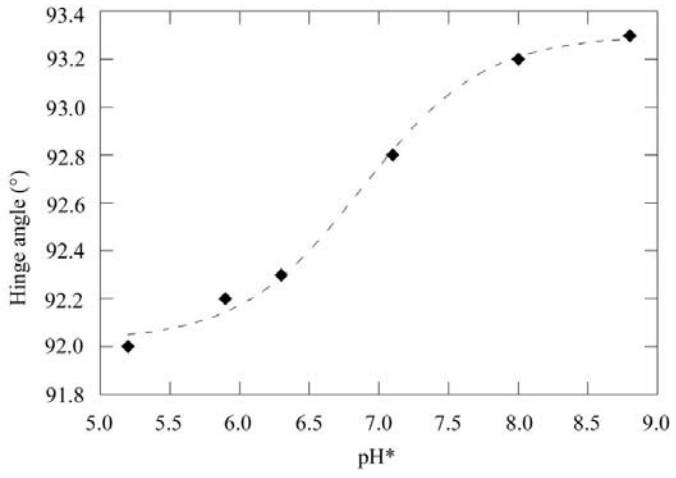

Figure 5
β-Structure rearrangement *versus* pH*. The hinge angle is formed by the lines joining the centres of mass of V_1 (residues 61–63, 71–75 and 105–111) and V_2 (residues 42–46, 82–87 and 96–101) to the centre of mass of the hinge elbow residues (47–48, 80–81 and 102–104) connecting V_1 and V_2.

The peculiar V-shaped motif of the RNase A tertiary fold is formed by the two antiparallel β-sheets, called V_1 and V_2, with the catalytic site located in the cleft between them. V_1 and V_2 are formed by residues 61–63, 71–75 and 105–111 and residues 42–46, 82–87 and 96–101, respectively. Sequential reorientations of the V_1 and V_2 arms are observed with an increase in pH*, thus leading to a subtle opening of the enzyme β-structure. Indeed, after superimposition of the V_2 arm of the six structures, a further rotation of the molecule is required to superimpose the V_1 arm. The reorientation of the two β-sheets was estimated by calculating the angle (hinge angle) formed by the lines joining the centres of mass of V_1 and V_2 to the centre of mass of the hinge elbow residues (47–48, 80–81 and 102–104) connecting V_1 and V_2. This angle increases from 92.0 to 93.3° with incresing pH* (Fig. 5). The values of the hinge angle at the two extremes of pH* compare well with the values calculated for the phosphate-free (PDB code 7rsa) and the sulfate-bound RNase A (PDB code 5rsa), which are 92.7 and 91.5°, respectively. As shown in Fig. 5, the hinge angles are clearly pH* dependent and show a sigmoidal trend with pH*. Water molecules bound to the V_1 and the V_2 arms appear to move consistently with the β-structure.

Changes of the tertiary structure owing to ligand binding have been frequently found in proteins (Hayward, 1999). In this context, we found in previous work that a small β-rearrangement in bovine seminal RNase (BS-RNase) (Vitagliano *et al.*, 1998) and in RNase A (Vitagliano *et al.*, 2002) led to a more compact structure upon binding. Similar motions had been previously observed, in RNase A, to depend on the content of protein hydration (Radha Kishan *et al.*, 1995; Sadasivan *et al.*, 1998).

In the present case, both the pH*-driven variations of the electrostatic potential and the release of the sulfate anion from the active site, two strictly correlated effects, concur to contribute to the tertiary structural changes observed. However, the former is likely to produce a closure of the enzyme at high pH*, as the active site remains uncharged (Fig. 4*b*). Therefore, the β-structural rearrangement found may be mainly ascribed to the release of the active-site-bound sulfate.

3.5. Disulfide bridge Cys65–Cys72: implications for protein folding

Disulfide bridges are critical to protein stability and there are only a few cases where they exhibit conformational flexibility (Czapinska *et al.*, 2000; Addlagatta *et al.*, 2001). RNase A is cross-linked by four disulfide bridges, two (Cys26–Cys84 and Cys58–Cys110) connecting α- and β-strands and the other two (Cys65–Cys72 and Cys40–Cys95) connecting external loops.

In contrast to the previously reported structures of RNase A, we found that the bridge involving Cys65 and Cys72 ([65–72]) exists in two well defined conformations (*A* and *B*), as shown in Fig. 6. The occurrence of the *A* and *B* conformations of the [65–72] disulfide bridge is not pH*-correlated, with occupancies of 80 and 20%, respectively. The conformational parameters of the four disulfide bridges of RNase A

are reported in Table 3. Since these parameters are similar in the six structures, only those belonging to the structure at the highest resolution (pH* 5.9) are listed. The bridges [26–84], [40–95] and [58–110] are classified (according to Richardson, 1981), as left-handed spiral conformations. In contrast, the most abundant *A* rotamer of the bridge [65–72] adopts a right-handed hook conformation (Richardson, 1981), whereas the *B* rotamer is left-handed.

Table 3
Disulfide-bond conformational parameters.

Values of φ, ψ and ω are reported for the upstream/downstream cystines, respectively. All parameters refer to the structure at the highest resolution (pH* 5.9).

Disulfide bridge	χ_1 (°)	χ_2 (°)	χ_3 (°)	χ'_2 (°)	χ'_1 (°)	$C^\alpha-C^\alpha$ (Å)	$C^\beta-C^\beta$ (Å)	φ (°)	ψ (°)	ω (°)
26–84	−71	−85	−79	−60	−58	5.66	3.62	−64/−120	−44/126	−176/178
40–95	−54	−56	−83	−71	−53	5.55	3.70	−78/−69	109/137	173/179
58–110	−60	−65	−85	−123	−56	5.98	3.76	−64/−119	−7/146	177/−178
65–72*A*	−52	−60	104	86	−75	5.26	4.04	−68/−97	166/154	168/175
65–72*B*	−86	83	−97	−141	−52	5.26	4.04	−68/−97	166/154	168/175

Recent statistics (Petersen *et al.*, 1999) based on 351 disulfide bridges in 131 non-homologous single-chain protein structures have shown that left- and right-handed bridges usually occur with a similar frequency in protein structures. However, left-handed bridges characterized by negative χ_2 and χ'_2 are particularly abundant. Left-handed bridges are usually characterized by larger $C^\alpha-C^\alpha$ distances between the half-cystines. As shown in Table 3, the conformations of the disulfide bridges [26–84], [40–95] and [58–110] of RNase A fall within this last category. Furthermore, right-handed bridges with negative χ_2 and positive χ'_2, as in the case of the *A* conformer of the [65–72] bridge, are not very frequent in proteins. Similarly, left-handed bridges with positive χ_2 and negative χ'_2, as for the *B* conformer of [65–72], are extremely rare.

The [65–72] bridge has been the object of several recent studies on RNase A folding and stability. Such studies have shown that the [65–72] bridge is the first to be formed along the folding pathway (Xu *et al.*, 1996), despite its poor contribution to protein stability (Klink *et al.*, 2000), and that its removal has no effects on the kinetics of folding (Ruoppolo *et al.*, 2000). On the other hand, folding kinetics are strongly influenced by structural alterations of the type III β-turn which encompasses residues 66–69 (Orrù *et al.*, 2000). In the present structures, the alternation of two scarcely populated (high-energy) conformations of the disulfide bridge [65–72] clearly indicate that the local conformation of the polypeptide chain is dictated by the formation of the energetically favourable local β-structure, rather than by the stereochemical requirements of the disulfide bridge. Interestingly, the loop [65–72] plays a key role in the substrate affinity and specificity (Harper & Vallee, 1989). Preservation of this loop conformation is essential, since any alterations of the molecule leading to a significant structural change of this loop would produce a significant decrease of the enzyme activity and binding (Allemann *et al.*, 1991).

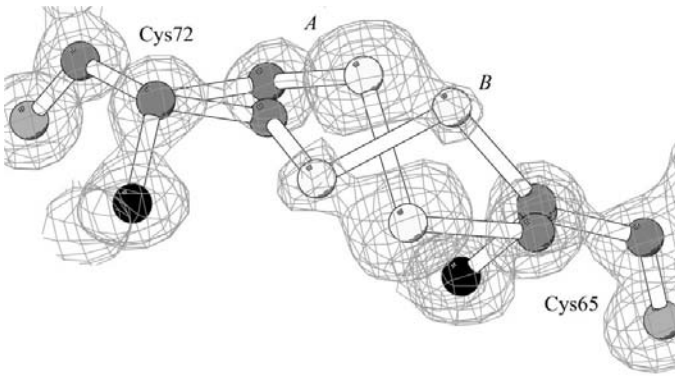

Figure 6
Electron-density map ($3F_o - 2F_c$), contoured at 2.7σ, showing the double conformation of the disulfide bridge [65–72].

Table 4
Number of conserved water sites.

Clustering radius (Å)	1.5	0.7	0.3
Sites found in all six structures	151	113	58
Sites found in five structures	174	140	74
Sites found in four structures	195	157	96

3.6. Solvent structure

Since well organized hydration patterns were observed for the six structures, a thorough analysis of the protein solvation was carried out. Conserved water molecules were identified using different clustering distances from the reference structure at the highest resolution (at pH* 5.9). As shown in Table 4, depending on the stringency of the radius used to define a cluster of equivalent sites a variety of numbers of water sites can be identified as conserved.

It is worth noting that using a clustering radius of 1.5 Å, about 64% of the fully occupied water sites are conserved in all of the six models (Table 4), whereas about 82% are conserved in four of the six models. The changes in the location of some water molecules may be ascribed to the pH* variations. For example, the distribution of the water molecules in the catalytic site is significantly different in the six structures. Indeed, four water molecules displace the sulfate ion at neutral pH* (Fig. 3*a*). Two of them hydrogen bind the catalytic His12 and His119 (W1 and W4 in Fig. 3*a*, respectively). In addition, in a region remote from the active site, the deprotonation of His48 at neutral pH* induces a conformational change in Gln101 which displaces two water molecules (Berisio *et al.*, 1999).

Using a very stringent radius of 0.3 Å, only 58 water sites (about 24% of the whole crystalline solvent content) are conserved. We found that these molecules are directly or indirectly bound to α-helices. The lower extent of conserved

water molecules bound to β-strands is likely to be a consequence of the subtle pH*-induced motion of the β-structure reported above. A major group (19 out of 58) surrounds the N-terminal segment (residues 1–22) filling all the solvent exposed clefts that surround it, this being in accordance with data reported by Lisgarten *et al.* (1993). These water molecules may be important to stabilize the most solvent-exposed N-terminal helix.

4. Conclusions

The results presented here highlight the dynamic properties of a protein structure as a function of pH*. The high quality of the six atomic resolution structures is indicated by the low estimated uncertainties of the atomic positions, by the possibility of seeing many H atoms in the electron-density maps and in particular by the observed correlation between the backbone geometrical parameters and the residue conformation. This correlation proved to be significant even in the presence of restraints which would act to stifle any variations. Such effects are therefore restraint-independent and may be used as tools to test protein structure refinement.

The high accuracy of the six models was a necessary requirement for the definition of subtle yet systematic variations of the protein structure as a function of pH*. Indeed, even at the level of the solvent molecules there is a substantial agreement of the crystal structures, which allows a number of real differences to be identified in an unambiguous way. These differences are not a result of crystal packing, since they occur under a strict invariance of packing interactions. Among the pH*-driven variations, the subtle rearrangement of the β-structure through the release of a sulfate anion from the active site is an unbiased observation of domain motions in proteins. Although small, such motions may gain a particular importance for protein function as the complexity of the system increases and may play a significant role in the cooperativity phenomenon of oligomeric systems (Vitagliano *et al.*, 1998, 1999).

The comparison of the active-site architectures has revealed a net structural change of the catalytic Lys41 in the pH* range 8.0–8.8, which has been associated with its deprotonation. At pH 8.8, the Lys41 side chain points towards the P2 site, in a conformation found to be strongly disfavoured, on the basis of electrostatic potential calculations, when the lysine is charged. This finding suggests that residues Lys7 and Arg10, belonging to the P2 site, may act to stabilize the catalytically active conformation of Lys41 by limiting its accessible conformational space, *i.e.* by disfavouring the conformations pointing outside the active-site pocket. Furthermore, our results suggest that Lys41 is very unlikely to act as a general base during catalysis, in contrast to the proposal of Wladkowski *et al.* (1998).

Finally, the six atomic resolution structures support a number of experimental data, indicating a low contribution of the disulfide bridge [65–72] to protein stability and the importance of the integrity of the local β-structure of the loop [65–72] for enzyme catalysis (Klink *et al.*, 2000; Orrù *et al.*, 2000; Ruoppolo *et al.*, 2000).

This work was supported by PRIN2000 and CNR 'Agenzia2000'. The authors are grateful to G. Sorrentino and to L. De Luca for technical assistance.

References

Addlagatta, A., Krzywda, S., Czapinska, H., Otlewski, J. & Jaskolski, M. (2001). *Acta Cryst.* D**57**, 649–663.
Allemann, R. K., Presnell, S. R. & Benner, S. A. (1991). *Protein Eng.* **4**, 831–835.
Ashida, T., Tsunogae, Y., Tanaka, I. & Yamane, T. (1987). *Acta Cryst.* B**43**, 212–218.
Berisio, R., Lamzin, V. S., Sica, F., Zagari, A., Wilson, K. S. & Mazzarella, L. (1999). *J. Mol. Biol.* **292**, 845–854.
Blackburn, P. & Moore, S. (1982). *The Enzymes*, Vol. 15, edited by P. D. Boyer, pp. 317–433. New York: Academic Press.
Czapinska, H., Otlewski, J., Krzywda, S., Sheldrick, G. M. & Jaskolski, M. (2000). *J. Mol. Biol.* **295**, 1237–1249.
Dauter, Z., Lamzin, V. S. & Wilson, K. S. (1997). *Curr. Opin. Struct. Biol.* **7**, 681–688.
Dixon, M. M., Brennan, R. G. & Matthews, B. W. (1991). *Int. J. Biol. Macromol.* **13**, 89–96.
Esnouf, R. M. (1999). *Acta Cryst.* D**55**, 938–940.
Esposito, L., Vitagliano, L., Sica, F., Sorrentino, G., Zagari, A. & Mazzarella, L. (2000). *J. Mol. Biol.* **297**, 713–732.
Esposito, L., Vitagliano, L., Zagari, A. & Mazzarella, L. (2000). *Protein Sci.* **9**, 2038–2042.
Fisher, B. M., Grilley, J. E. & Raines, R.T. (1998). *J. Biol. Chem.* **273**, 34134–34138.
Fisher, B. M., Ha, J.-H. & Raines, R. T. (1998). *Biochemistry*, **37**, 12121–12132.
Fisher, B. M., Schultz, L. W. & Raines, R. T. (1998). *Biochemistry*, **37**, 17386–17401.
Gilson, M. K. & Honig, B. H. (1987). *Nature (London)*, **330**, 84–86.
Gursky, O., Badger, J., Li, Y. & Caspar, D. L. D. (1992). *Biophys. J.* **63**, 1210–1220.
Harper, J. W. & Vallee, B. L. (1989). *Biochemistry*, **28**, 1875–1884.
Hayward, S. (1999). *Proteins*, **36**, 425–435.
Honig, B. H. & Nicholls, A. (1995). *Science*, **268**, 1144–1149.
Jeffrey, G. A., Houk, K. N., Paddon-Row, M. N., Rondan, N. G. & Mitra, J. (1985). *J. Am. Chem. Soc.* **107**, 321–326.
Jones, T. A., Zou, J. Y., Cowan, S. W. & Kjeldgaard, M. (1991). *Acta Cryst.* A**47**, 110–119.
Kabsch, W. & Sander, C. (1983). *Biopolymers*, **22**, 2577–2637.
Karplus, P. A. (1996). *Protein Sci.* **5**, 1406–1420.
Klink, T. A., Woycechowski, K. J., Taylor, K. M. & Raines, R. T. (2000). *Eur. J. Biochem.* **267**, 566–572.
Knoblauch, H., Rueterjans, H., Bloemhoff, W. & Kerling, K. E. T. (1988). *Eur. J. Biochem.* **172**, 485–497.
Lisgarten, J. N., Gupta, V., Maes, D., Wyns, L., Zegers, I., Palmer, R. A., Delawis, C. G., Aguilar, C. F. & Hemmings, A. M. (1993). *Acta Cryst.* D**49**, 541–547.
Lublowski, J., Dauter, Z., Yang, F., Alexandratos, J., Merkel, G., Skalka, A. M. & Wlodawer, A. (1999). *Biochemistry*, **38**, 13512–13522.
Nicholls, A. & Honig, B. H. (1991). *J. Comput. Chem.* **12**, 435–445.
Nogues, M. V., Moussaoui, M., Boix, E., Vilanova, M., Ribò, M. & Cuchillo, C. M. (1998). *Cell Mol. Life Sci.* **54**, 766–774.
Orrù, S., Vitagliano, L., Esposito, L., Mazzarella, L., Marino, G. & Ruoppolo, M. (2000). *Protein Sci.* **9**, 2577–2582.
Park, C., Schultz, L. W. & Raines, R. T. (2001). *Biochemistry*, **40**, 4949–4956.

Petersen, M. T. N., Johnson, P. H. & Petersen, S. B. (1999). *Protein Eng.* **7**, 535–548.
Radha Kishan, K. V., Chandra, N. R., Sudarsanakumar, C., Suguna, K. & Vijayan, M. (1995). *Acta Cryst.* D**51**, 703–710.
Richardson, J. S. (1981). *Adv. Protein Chem.* **34**, 167–339.
Ruoppolo, M, Vinci, F, Klink, T. A., Raines, R. T. & Marino, G. (2000). *Biochemistry*, **39**, 12033–12042.
Sadasivan, C., Nagendra, H. G. & Vijayan, M. (1998). *Acta Cryst.* D**54**, 1343–1352.
Santoro, J., Gonzales, C., Bruix, M., Neira, J. L., Nieto, J., Herranz, J. L. & Rico, M. (1993). *J. Mol. Biol.* **229**, 722–734.
Sheldrick, G. M. & Schneider, T. R. (1997). *Methods Enzymol.* **276**, 319–343.
Tilton, R. F., Dewan, J. C. & Petsko, G. A. (1992). *Biochemistry*, **31**, 2469–2481.
Vitagliano, L., Adinolfi, S., Riccio, A, Sica, F., Zagari, A. & Mazzarella, L. (1998). *Protein Sci.* **7**, 1691–1699.
Vitagliano, L., Adinolfi, S., Sica, F., Merlino, A., Zagari, A. & Mazzarella, L. (1999). *J. Mol. Biol.* **293**, 569–577.
Vitagliano, L., Merlino, A., Zagari, A. & Mazzarella, L. (2002). *Proteins*, **46**, 97–104.
Wladkowski, B. D., Svensson, L. A., Sjölin, L., Ladner, J. E. & Gilliland, G. L. (1998). *J. Am. Chem. Soc.* **120**, 5488–5498.
Wlodawer, A., Svensson, L. A., Sjölin, L. & Gilliland, G. L. (1988). *Biochemistry*, **27**, 2705–2717.
Xu, X., Rothwarf, D. M. & Scheraga, H. A. (1996). *Biochemistry*, **35**, 6406–6417.
Yang, F. & Phillips, N. Jr (1996). *J. Mol. Biol.* **256**, 762–774.